Nanoscale

Accepted Manuscript

Table of contents:

Photosensitizer methylene bluewas confined to the close vicinity of the Au nanorod, by incorporating it into SiO_2 during the Au-core/SiO_2-shell nanoparticle growth. Upon light irradiationof the nanoparticles, generation of reactive oxygen species and their transport to the cytoplasma were visualized in vitro, and they were found to be directly responsible for the significantly decreased cell viability.

Keywords: silica, gold, nanoparticle, SPR, ROS

Surface plasmon enhanced drug efficacy using core shell Au@SiO_2 nanoparticle carrier

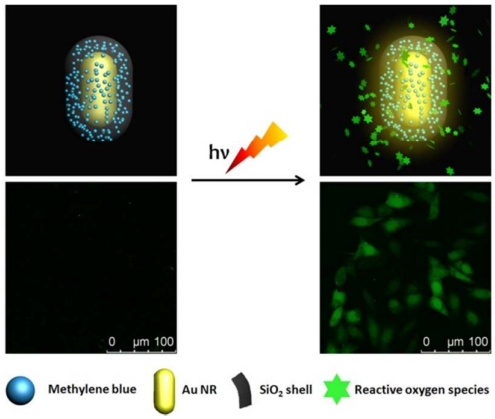

Cite this: DOI: 10.1039/c0xx00000x

www.rsc.org/xxxxxx

ARTICLE TYPE

Surface plasmon enhanced drug efficacy using core shell Au@SiO_2 nanoparticle carrier

Zhiqin Chu[a], Chun Yin[b], Silu Zhang[a], Ge Lin[b,*], Quan Li[a,*]

Received (in XXX, XXX) XthXXXXXXXXX 20XX, Accepted Xth XXXXXXXXX 20XX

DOI: 10.1039/b000000x

Photosensitizer (PS) methylene blue (MB) is confined to the close vicinity of the Au nanorod, by incorporating it into SiO_2 during the Au-core/SiO_2-shell nanoparticle (NP) growth. Upon light irradiation of the Au@(SiO_2-MB) NPs, generation of reactive oxygen species and their transport to the cytoplasma are directly responsible for the significantly decreased cell viability. We have excluded the independent role of photothermal effect and demonstrated the major role of plasmonic effect in enhancing drug efficacy using Au@(SiO_2-MB) NPs. The "spatial vicinity" required for Au and the PS and the "energy match" between the PS absorption and Au surface plasmon resonance are two critical factors to enable the plasmonic effect, which leads to enhanced drug efficacy.

Introduction

In the recent years, several nanoparticulate systems, including polymeric[1], metallic[2] and silica-based nanoparticles (NPs)[3], have demonstrated good biocompatibility, and thus are considered as drug carriers, aiming at enhanced drug bioavailability and efficacy[4]. Among various possible carrier choices, silica NPs have advantages of easily modifiable surface chemical characteristics and excellent stability in physiological environment. In addition, it has been reported to effectively enter the cell interior via endocytosis process[5]. Its biocompatibility makes it as one of the most promising drug carrier candidates[6]. Several different mechanisms[3, 7, 8]are found to be effective in loading the drugs in SiO_2 NPs, and the loading capacity is reported to be satisfactory[6, 9]. Another interesting candidate for drug carrier is Au NP. Its unique properties upon light irradiation, such as surface plasmon resonance (SPR), bring in additional advantages to improve the drug efficacy[2, 10, 11]. It has been reported that the yield of the triplet states[12] and consequently singlet oxygen (one type of reactive oxygen species (ROS)) generation from the drug can be enhanced by attaching the molecules to the metallic NP surface[13]. Nevertheless, evidence of the improved drug efficacy directly gained from via plasmonic effect is rare. In fact, effective loading of the drugs to the Au NP remains as a problem. Most of the loading is realized by depositing the drug molecules on the surface of the Au NP[2, 14]with limited loading capacity[1]. In such a configuration, the drug molecules remain exposed to the physiological environment.

In the present study, we have combined advantages of both SiO_2 and Au NPs by designing Au-core/SiO_2-shell nanocarriers with drug molecule embedded in the SiO_2 shell layer, which served as the stable host matrix. Au nanorod (NR), was chosen as the core, making it possible to adjust the plasmon resonance energy by changing its aspect ratio[15]. Methylene blue (MB), a drug with a wide range of therapeutic applications (including malaria[16], alzheimer disease[17], methemoglobinemia[18] and etc.) and also a commonly used photosensitizer (PS)[19], was chosen as a model molecule to be incorporated into the silica shell of the Au@SiO_2 NPs. By spatially confining the drug in the vicinity of the Au core and tuning the Au SPR energy to match its absorption energy, we unambiguously demonstrate enhanced drug efficacy with the mechanism elaborated for such enhancement.

Results and discussions

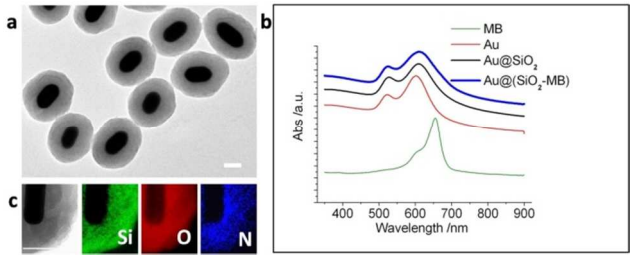

Fig.1 (a) Low magnification TEM image of the Au@(SiO_2-MB)NPs. (b) Absorption spectra taken from MB alone, Au NRs, Au@SiO_2 NPs, and Au@(SiO_2-MB) NPs in aqueous solution ([MB] = 5 μM for all samples). (c) Low magnification TEM image taken from part of one Au@SiO_2 NP and the corresponding EELS maps of Si (green), O (red) and N (blue). The scale bar is 50 nm.

Figure 1a showed a typical TEM image of the Au@ (SiO_2-MB) NPs. The Au NR core had an average diameter of ~40 nm and an aspect ratio close to 2. The silica-MB shell appeared uniform with a thickness of ~40 nm. The Au NR itself had two plasmonic absorption peaks (Fig. 1b) with the transverse mode occurring at ~522 nm, and longitudinal mode at longer wavelength, which was tunable by varying the aspect ratio of the NR (~ 2 in the present case, so that the longitudinal plasmon resonance wavelength was controlled at ~600 nm). When the SiO_2 (without MB) shell was introduced, a small red shift of the longitudinal mode to ~610 nm would occur due to the larger refractive index of the SiO_2 as the

View Article Online

surrounding medium[20](Fig. 1b). On the other hand, MB itself normally had two absorption peaks at 665nm and 600nm[21], corresponding to monomer and dimer absorptions, respectively (Fig. 1b). Incorporating MB into the SiO_2shell seemed not affect the original absorption characteristic of the Au@SiO_2 NPs (without MB), but only a slight broadening of the longitudinal SPR absorption of the Au (Fig. 1b). This was due to the energy overlapping of the MB absorptions and the Au longitudinal SPR. One should note that the Au@(SiO_2-MB) NPs was synthesized in the alkaline environment, which induced successive demethylation of MB, leading to reduced monomer absorption[22] and increased dimer absorption once they were embedded in the SiO_2 shell (Fig. S2). By manipulating the Au NR's aspect ratio and thus shifting the Au longitudinal SPR away from 600nm, the MB absorption can be observed (Fig. S3). Further support of MB being incorporated into the SiO_2 shell came from the elemental maps of Si, O, and N taken from one such core/shell NP (Fig. 1c). The observation of N in the SiO_2 shell suggested the presence of MB, as it is a compositional element of MB but not SiO_2.

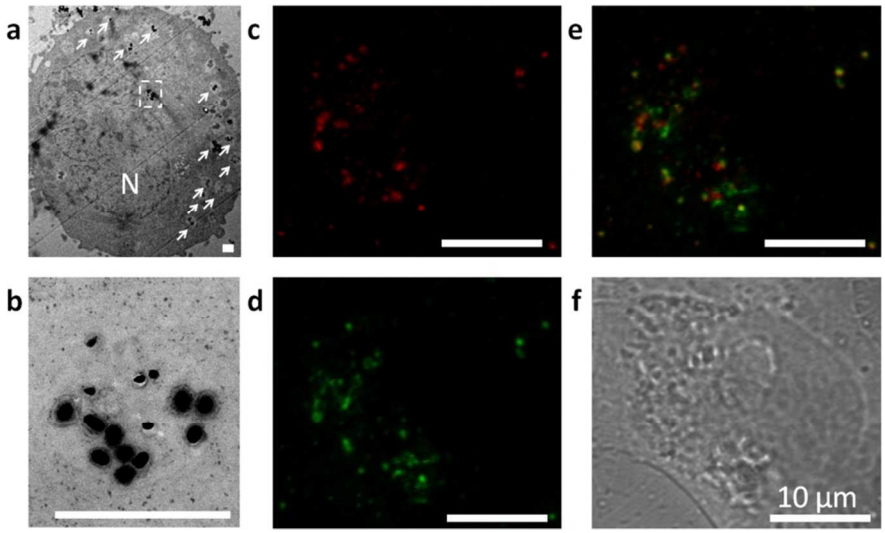

Fig. 2 Intracellular localization of Au@ (SiO_2-MB) NPs inside HepG2 cells.(a) TEM image showing one of the HepG2 cells treated with Au@(SiO_2-MB) NPs for 24 hours. NPs residing inside the cells can be observed (marked by arrows).(b) Magnified TEM image of the boxed region in Figure 2a. (The scale bar is 500 nm, N stands for "nucleus" in the cell). Confocal microscopy images showing the localization of Au@(SiO_2-MB) NPs inside one typical HepG2 cell. (c) Fluorescence signal (red color) from MB in the cell fed with Au@(SiO_2-MB) NPs. (d) Two photon luminescence (TPL) signal (green color) from Au in the cell fed with Au@(SiO_2-MB) NPs. (e) Color map obtained by overlapping (c) and (d), disclosing the spatial distribution of MB and Au in the cell. The significant signal overlap between MB fluorescence and Au TPL suggests that MB is mainly confined in the vicinity of the Au. (f) Transmittance image showing the morphology of the specific HepG2 cell used in (c)-(e).

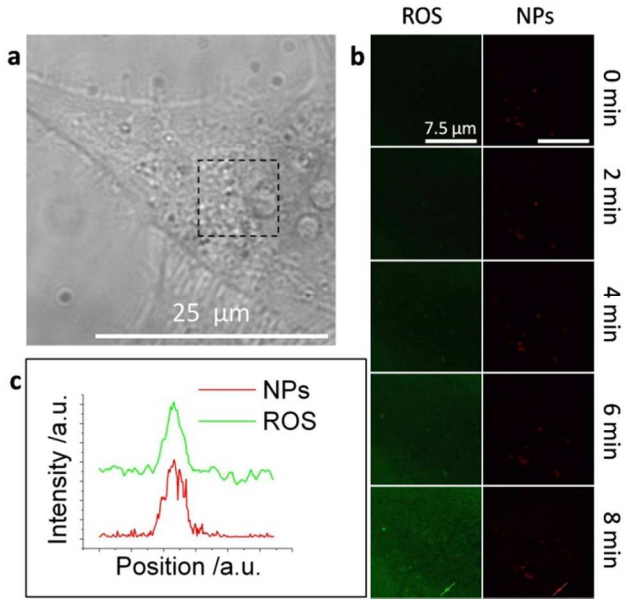

Fig. 3 Monitoring of ROS generation in one typical HepG2 cell incubated with Au@(SiO_2-MB) NPs. (a) Transmittance image showing part of the HepG2 cell. The boxed region was chosen for real-time monitoring of ROS generation after the cells' being incubated with Au@(SiO_2-MB) NPs for 24 hours. (b) Evolution of the ROS level as a function of the observation time. The ROS signal was measured by carboxy-H_2DFFDA. The NP locations in the

corresponding region were determined using the MB fluorescence signal (red color). Excitation of the MB molecules occurred during the confocal imaging process due to laser beam irradiation. (c) Intensity profile of green line and red line in Figure 3b, showing good correlation between the NP position and the highest ROS signal.

Similar to SiO_2 NPs[5], the Au@(SiO_2-MB) NPs were found to enter the cell interior (Fig. 2a) easily via endocytosis, i.e., they were always found in membrane bounded organelles (Fig. 2b) in the cytoplasma—a direct consequence of the endocytosis process. This was further confirmed by confocal microscopy results (Fig. S4). The amount of NPs uptaken by the cells was found to increase with prolonged incubation periods (Fig. S5). Excellent correlation between the location of Au and MB was evidenced in studying their distribution by confocal microscopy (Fig. 2c-2f). We found that most of the florescence signal of MB overlapped (Mander's overlap coefficient[23] was determined as 0.717 by ImageJ) with that of the Au during the whole observation period (24 hours). This results also coincided with our MB leaching test experiment, in which only ~10% of MB has been leaked from the Au@(SiO_2-MB)NPs after 24 hours' incubation in DMEM medium at 37 ^oC. (Table S1). Together with the EELS elemental mapping of such nanoparticles (Fig. 1c), the above results suggested that the most of the MB molecules were confined in the vicinity of the Au core.

Under light irradiation, it is known that the excited PS drug molecules interact with chemicals in the surrounding environment to produce ROS, which is responsible for cell damages[24]. We then compared the ROS generation capability of MB, SiO_2-MB NPs, and Au@(SiO_2-MB) NPs in aqueous solution respectively. Singlet oxygen, hydroxyl radical and superoxide are three major types of ROS commonly tested[25]. Upon light irradiation on the aqueous solution of the three for 20 minutes, the Au@(SiO_2-MB) NPs was found to generate more hydroxyl radical and superoxide than the other two (both free MB and SiO_2-MB NPs), while free MB led to the most singlet oxygen production among the three (Fig. S6). The intracellular ROS signal, which was examined using carboxy-H_2DFFDA (ROS detection dye, responding to all types of ROS), were found to be high in the Au@(SiO_2-MB) NPs treated cells, but barely discernable in those incubated with Au@SiO_2 NPs (without MB) (Fig. S7). Although we have shown earlier that MB was mainly confined inside the silica matrix, such confinement did not apply to the photo-generated ROS. Obviously ROS was always firstly generated around the MB molecules (i.e., in the vicinity of Au NRs cores where MB was confined to (Fig. 2c-2f)), they were then found to diffuse out and be dispersed in the cytoplasma, as evidenced in our time-dependent confocal experiments of tracing the ROS in the NP-treated cells (Fig.3). We found that the ROS level was always the highest where the Au@(SiO_2-MB) NPs were. This can be seen by correlating the fluorescence intensity peak position of the ROS and the MB signal (given that most of the MB were trapped in the nanocarrier (Fig. 2c-2f)), as shown in the plot in Figure 3c. Nevertheless, the ROS level in the cytoplasma, where the Au@(SiO_2-MB) NPs were absent, continuously increased with the time (Fig.3b), as more and more ROS were released into the cytoplasma from the Au@(SiO_2-MB) NPs. It is also important to note that at the end of 8 minutes' observation, the total amount of ROS generated by the Au@(SiO_2-MB) NPs was much more than that of free MB (Fig. S8), as suggested by the florescence intensity of the ROS detection dye.

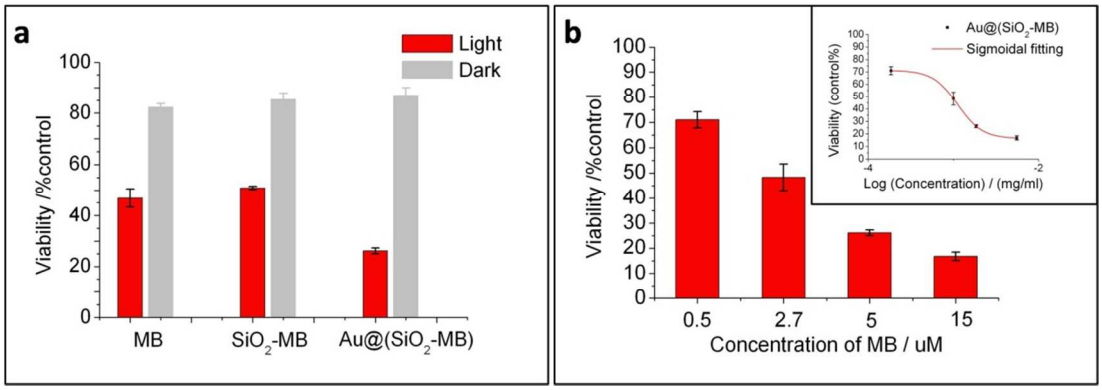

Fig. 4 Efficacy comparison of Au@(SiO_2-MB) NPs and MB alone incubated with HepG2 cells by MTT assay. (a) Viability of the HepG2 cells incubated with MB, SiO2-MB and Au@(SiO_2-MB) NPs for 24 hours. The concentration of MB is kept at 5 μM for all samples examined. (b) MB concentration dependence of the HepG2 cells viability when being incubated with Au@(SiO_2-MB)NPs for 24 hours, the upper right insert is the sigmoidal fitting of the obtained viability curve. The feeding concentration of the NPs is kept the same for all experiments. Data are presented with mean ± standard deviation (SD) from three independent experiments. All data were shown as mean ± SD (from three independent experiments) and significantly different ($p < 0.05$) from control (analyzed by Student's t test). The R^2 of sigmoidal fitting was 0.99.

The efficacy of the drug with and without specific nanocarriers were further investigated by irradiating the drug-fed cells with light emitting diode (LED), followed by measuring the viability of the cells using 3-(4,5-Dimethylthiazol-2-yl)-2,5-diphenyltetrazolium bromide (MTT) assay. Cells treated with MB alone at different concentration were firstly examined, and the IC_{50} of MB (the concentration produces 50% viability) was determined as 4.70±0.07μM (Fig.S9). Therefore, for the simple and direct comparisons, 5μM of MB were used in the later experiments. The viability of the cells were then compared

among the treatments with MB alone, SiO_2-MB NPs (Fig. S2), and Au@(SiO_2-MB) NPs (Fig. 4a). Low cytotoxicity (~85%viability) was observed when cells were treated with MB, SiO_2-MB and Au@(SiO_2-MB) in dark. After 590 nm LED irradiation for 20 minutes, the cell viability dropped to, 47%, 51%, and 26%, for MB, SiO_2-MB NPs and Au@(SiO_2-MB)NPs treated cells, respectively. The concentration dependent effect of Au@(SiO_2-MB) NPs was demonstrated in the core/shell nanocarriers as illustrated in Figure 4b. Furthermore, comparing with MB alone (IC_{50} was 4.70 μM (Fig. S9)), Au@(SiO_2-MB) significantly enhanced the effect with IC_{50} of 2.59 μM.

The enhanced drug efficacy cannot be attributed to the enhanced cellular uptake of drug molecule (MB). We have carried out parallel experiments using SiO_2NPs with MB molecules incorporated. Such NPs were similar to the Au@(SiO_2-MB) NPs, as they shared the similar size and surface chemistry. The only difference was the absence of Au NR-core in SiO_2-MB NPs. MTT results suggested that such SiO_2-MB NPs failed to bring in any drug efficacy enhancement (Fig. 3a), although improved cellular uptake[26, 27]was similar to that of the Au@(SiO_2-MB) NPs. Therefore, the observed improvement must relate to the presence of Au NRs core. Photothermal effect had been demonstrated in the literature as an effective means to terminate cancer cells[28]. However, this can be excluded in the present study, as the energy density of LED light (irradiation source) was only 5 mW/cm^2, being several order of magnitude lower than that required to induce photothermal effect[28, 29]. A control experiment had also been conducted by comparing the viability of cells treated with Au@SiO_2NPs (without MB) before and after light irradiation. No significant differences in the cell viability were observed before (~87%) and after (~84%) LED irradiation (Fig. S10).

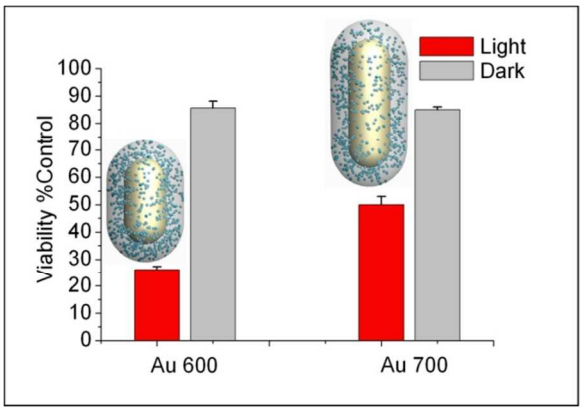

Fig. 5 Comparison of the HepG2 cells' viability (by MTT assay), when they were incubated (for 24 hours) with Au@(SiO_2-MB) NPs, in which the Au NR cores are of different aspect ratio. The corresponding longitudinal mode of Au SPR wavelength is 600 nm for Au600, and 700 nm for Au700, respectively. The concentration of MB is 5 μM for both of the samples. All data were shown as mean ± SD(from three independent experiments) and significantly different ($p < 0.05$) from control (analyzed by Student's t test).

We attribute the improved drug efficacy to plasmonic enhancement effect of the Au NRs core. When the Au SPR was excited, the intensified electromagnetic field in the vicinity of Au would contribute to the enhanced absorption of the PS drug molecules[30] and consequently led to the enhancement of drug efficacy. For such plasmonic enhanced effect, a match between the SPR energy and the excitation energy of the PS molecule must be reached in order to maximize the enhancement. In this regard, we prepared another batch of Au@(SiO_2-MB) NPs, in which the longitudinal SPR of Au occurred at ~700nm (Fig. S3), being away from the MB absorption energy, i.e., 600nm for dimer (majority in the SiO_2 shell) and 665 nm for monomer. The photodynamic activity of the two different kinds of Au@(SiO_2-MB) NPs (denoted as Au600 and Au700, respectively)in HepG2 cells were further tested by the MTT assay and the results were shown in Figure5. After being irradiated by the 590 nm LED for 20 minutes, the viability of the Au600 treated cells dropped to 26%, while 50%viability were found in the cells treated with the Au700 (Fig. 5).

Another criterion for SPR enhanced efficacy is that the PS molecules must be located in the close vicinity of the Au NRs core. It is known that the plasmonic effect decay drastically with the distance away from the Au surface. In this regard, confining the drug inside the SiO_2 shell is a necessity to achieve the plasmonic enhancement. Indeed, the MB had always been found around the Au core, as proved by the overlapped fluorescence signal from MB and Au in confocal microscopy (Fig. 2). By simultaneously introducing MB and Au NR into the cells failed to result in any significant drug efficacy enhancement, further supporting the above argument (Fig. S11).

Conclusions

We gave direct experimental evidence that plasmonic effect can be an effective mechanism for enhanced drug efficacy. By incorporating MB into SiO_2 during Au-core/SiO_2-shell NP growth, we obtained the Au@(SiO_2-MB) NPs, which demonstrated efficient cellular uptake via endocytosis. We found that the light irradiation caused ROS was firstly generated in the vicinity and then diffused out of NP in a time dependent manner, being responsible for the cell death. Stable spatial confinement of the MB in the close vicinity of the Au NR core and the energy match between the MB absorption and Au SPR are criteria in enabling the Au plasmonic effect for enhanced drug efficacy. Together with the biocompatibility of SiO_2 itself, the present work suggests a promising nanocarrier system for cancer therapeutics.

Experimental section

Preparation of Au@(SiO_2-MB)NPs

The growth of the Au NRs was firstly conducted using a seed-mediated method[31]. The as-grown NR can be shortened by oxidation[32], resulting different NR aspect ratios and thus their SPR energy. Pegylation of Au NR (40 ml) was realized by mixing them with freshly prepared aqueous mPEG-SH solution (1 mM, 2 ml; NANOCS, America) in 30^{o}C water bath overnight. Growth of the Au@(SiO_2-MB) NPs was similar to that of Au@SiO_2 NPs reported in the literature[33]. A thin layer of SiO_2 was firstly grown on the Au NR surface before MB (chosen as the photodynamic therapy (PDT) drug in the present study) was incorporated during further silica shell growth onto the as-prepared Au@SiO_2 NR. The thickness optimization of the thin SiO_2 layer on the Au NR before MB incorporation was illustrated

in Figure S12. The detailed synthesis process can be found in the following: In a typical procedure, 7.5 ml as-prepared Au@SiO_2 NRs were mixed with 2.3 ml deionized H_2O and 0.15 ml 30% ammonia-water solution, after which 50 µl MB stock solution (10 mM in ethanol) was added before 20 µl TEOS was finally introduced. The resulted NPs were washed and dried at 65°C for further use. As a control sample, the SiO_2-MB NPs were synthesized based on the conventional method that has been published elsewhere[22]. Typically, 0.34 ml MB stock solution (10 mM in ethanol) was firstly added to a mixture of 75 ml ethanol with 7 ml 30% ammonia-water solution, after which 0.4 ml TEOS was added. The SiO_2-MB NPs were obtained after 2 hours' reaction, and washed several times before their being dried.

The general morphology, size, and the size distribution of the NPs were characterized using transmission electron microscopy (TEM, Philips CM120). The electron energy-loss spectroscopy (EELS) was performed in TEM (Tecnai G2, FEG) attached with a Gatan imaging filtering (GIF) system. The chemical maps of the compositional elements (with beam energy at 200 KV, spot size 1, Gun lens 1, binning by 2, dwell time ~ 5 seconds for Si, 12 seconds for O and 20 seconds for N) were obtained at the Si L edge (at 99 eV), O K edge (at 532 eV), and the N K edge (at 401 eV). All of the UV/Vis absorption spectra were acquired using HitachiU-3501UV-visible-NIR spectrophotometer.

Quantifying various ROS generation in cuvette

To study ROS generation in cuvette, three different reagents were selected to detect the singlet oxygen (singlet oxygen sensor green (SOSG), Ex: 488 nm), hydroxyl radical (terephthalic acid (TA), Ex: 315 nm) and superoxide (dihydroethidium (DHE), Ex: 470 nm), respectively. The free MB, SiO_2-MB NPs or Au@(SiO_2-MB) NPs were respectively dispersed in cuvette with deionized water, followed by addition of proper amount of the specific ROS detection dye, and then irradiated with 590 nm LED (emission profile is shown in FigureS13 in supporting information) light for 20 minutes. Finally, the fluorescence signals of different ROS detection dyes in the cuvette were measured by a fluorescencespectrophotometer (Hitachi, FL7000). In all experiments, deionized water containing only the corresponding ROS detection dyes were used as the controls.

Introduce the Au@(SiO_2-MB) NPs to the cells

The HepG2, human liver carcinoma cells, were cultured in Dulbecco's modified Eagle's medium (DMEM), supplemented 10% heat-inactivated Fetal bovine serum (FBS), 2.0 g/L sodium bicarbonate, 0.1 g/L streptomycin sulfate, 0.06 g/L penicillin G and 5.958 g/L HEPES. The cells were maintained in a standard, cell culture incubator at 37°C in a humidified atmosphere with 5 % CO_2. All of the NPs were sterilized by steaming at 115℃ (NPs in powder form) for 2 hours, before they were dispersed in the medium and introduced to the cells, which had already been seeded and incubated for 24 hours. The concentration of NPs used in this study can be represented by that of Au NRs, which was calculated to be 0.34 nM from its UV/Vis absorption[34].

A home-built 590 nm LED was employed for the in *vitro* PDT study. The LED was aligned directly under the sample wells (96-well plates) to obtain uniform irradiation of the cells. The power density of the LED is 5 mW/cm^{-2}, which is too weak to cause any irradiation damage to the cells (Fig. S14).

Characterizations of the cells

For all transmission electron microscopy studies, the NP-fed cells were fixed with typical procedures published elsewhere[5]. Microtome (Leica, EM UC6) was then used to cut the cured cell cube (in Spurr resin (Electron microscopy sciences, USA)) into thin slices (70-90 nm in thickness). The samples were collected on 300-mesh copper TEM grids for observation.

For all confocal microscopy studies, the NP-fed cells wereeither kept alive or fixed with 4% paraformaldehyde at room temperature, before their being observed using confocal laser scanning microscopy (TCSP5, Leica) with a 63 × water-immersion objective lens at 633 nm excitation and 650 nm - 700nm emission.The TPL signal of Au NR (Fig. S15) was obtained by switching the light source to the near-infrared range using a two photon laser (Maitai, Spectra Physics in USA) and collecting the excitation signals in the green color channel (500 nm–550nm). To avoid signal overlapping with MB emission (~680nm), the TPL acquisition window was set at 500-550 nm. Finally, MB (red fluorescence) and Au NR (green fluorescence) images were merged and analyzed by using ImageJ software (National Institutes of Health,USA).

The intracellular ROS generation was studied using carboxy-H_2DFFDA (Invitrogen). Briefly, the cells were incubated with medium containing 5µM carboxy-H_2DFFDA for 50 minutes, before they were exposed to 590 nm LED for 20 minutes (excitation of the MB), followed by another 40 minutes incubation. The intracellular ROS level investigation was carried out using confocal microscope (TCSP5, Leica). The time dependent intracellular ROS generating process was investigated using live cells with the 633 nm and 488 nm laser as the irradiation source simultaneously, so that both MB and the ROS detection dye can be excited at the same time.

The cell viability was measured 24 hours after irradiation using MTT assay. The 24 hours delay was designed to account for both apoptosis and necrosis mechanisms of cell death[35]. The significance of all data was determined by Student's t-test for all in vitro studies, $p<0.05$ was deemed as significant for all data compared to control. IC_{50} values were determined from the mean results by plotting the logarithm of the MB concentration against cellular viability. The resulting curve was fit by a sigmoidal fit (Boltzman fit). The quality of the fitting can be evaluated by the coefficient of determination(R^2).

Acknowledgement

The authors are grateful to support from GRF of HKSAR (Project No. 414710).

[a]*Department of Physics, The Chinese University of Hong Kong, Shatin, New Territories, Hong Kong. E-mail: liquan@phy.cuhk.edu.hk*
[b]*School of Biomedical Sciences, Faculty of medicine, The Chinese University of Hong Kong, Shatin, New Territories, Hong Kong. E-mail: linge@cuhk.edu.hk*

† Electronic Supplementary Information (ESI) available:SeeDOI: 10.1039/b000000x/

References

1.H. J. Hah, G. Kim, Y. E. K. Lee, D. A. Orringer, O. Sagher, M.A.Philbert and R. Kopelman, Macromolecular Bioscience, 2011, **11**, 90-99.
2.M. K. K. Oo, X. Yang, H. Du and H. Wang, Nanomedicine, 2008, **3**, 777-786.
3.H. S. Qian, H. C. Guo, P. C. L. Ho, R. Mahendran and Y. Zhang, Small, 2009, **5**, 2285-2290.
4.P. Couleaud, V. Morosini, C. Frochot, S. Richeter, L. Raehm and J. O. Durand, Nanoscale, 2010, **2**, 1083-1095.
5.Z. Q. Chu, Y. J. Huang, Q. Tao and Q. Li, Nanoscale, 2011, **3**, 3291-3299.
6.I. Roy, T. Y. Ohulchanskyy, H. E. Pudavar, E. J. Bergey, A. R. Oseroff, J. Morgan, T. J. Dougherty and P. N. Prasad, Journal of the American Chemical Society, 2003, **125**, 7860-7865.
7.B. Z. Zhao, J. J. Yin, P. J. Bilski, C. F. Chignell, J. E. Roberts and Y. Y. He, Toxicology and Applied Pharmacology, 2009, **241**, 163-172.
8.H. L. Tu, Y. S. Lin, H. Y. Lin, Y. Hung, L. W. Lo, Y. F. Chen and C. Y. Mou, Advanced Materials, 2009, **21**, 172-177.
9.W. Tang, H. Xu, R. Kopelman and M. A. Philbert, Photochemistry and Photobiology, 2005, **81**, 242-249.
10.Y. Cheng, J. D. Meyers, A. M. Broome, M. E. Kenney, J. P. Basilion and C. Burda, Journal of the American Chemical Society, 2011, **133**, 2583-2591.
11.A. M. Fales, H. Yuan and T. Vo-Dinh, Langmuir, 2011, **27**, 12186-12190.
12.N. L. Pacioni, M. Gonzalez-Bejar, E. Alarcon, K. L. McGilvray and J. C. Scaiano, Journal of the American Chemical Society, 2010, **132**, 6298-6299.
13.Y. Zhang, K. Aslan, M. J. R. Previte and C. D. Geddes, Proceedings of the National Academy of Sciences of the United States of America, 2008, **105**, 1798-1802.
14.Y. Cheng, A. C. Samia, J. Li, M. E. Kenney, A. Resnick and C. Burda, Langmuir, 2010, **26**, 2248-2255.
15.B. Nikoobakht and M. A. El-Sayed, Chemistry of Materials, 2003, **15**, 1957-1962.
16.B. Coulibaly, A. Zoungrana, F. P. Mockenhaupt, R. H. Schirmer, C. Klose, U. Mansmann, P. E. Meissner and O. Muller, Plos One, 2009, **4**, e5318.
17.M. Oz, D. E. Lorke and G. A. Petroianu, Biochemical Pharmacology, 2009, **78**, 927-932.
18.R. H. Schirmer, H. Adler, M. Pickhardt and E. Mandelkow, Neurobiology of Aging, 2011, **32**, e7-e16.
19.X. X. He, X. Wu, K. M. Wang, B. H. Shi and L. Hai, Biomaterials, 2009, **30**, 5601-5609.
20.L. M. Liz-Marzan, M. Giersig and P. Mulvaney, Langmuir, 1996, **12**, 4329-4335.
21.K. Patil, R. Pawar and P. Talap, Physical Chemistry Chemical Physics, 2000, **2**, 4313-4317.
22.D. B. Tada, L. L. R. Vono, E. L. Duarte, R. Itri, P. K. Kiyohara, M. S. Baptista and L. M. Rossi, Langmuir, 2007, **23**, 8194-8199.
23.E. M. M. Manders, F. J. Verbeek and J. A. Aten, Journal of Microscopy-Oxford, 1993, **169**, 375-382.
24.C. A. Robertson, D. H. Evans and H. Abraharnse, Journal of Photochemistry and Photobiology B-Biology, 2009, **96**, 1-8.
25.M. Valko, D. Leibfritz, J. Moncol, M. T. D. Cronin, M. Mazur and J. Telser, International Journal of Biochemistry & Cell Biology, 2007, **39**, 44-84.
26.Slowing, II, B. G. Trewyn and V. S. Y. Lin, Journal of the American Chemical Society, 2007, **129**, 8845-8849.
27.Slowing, II, B. G. Trewyn, S. Giri and V. S. Y. Lin, Advanced Functional Materials, 2007, **17**, 1225-1236.
28.X. H. Huang, I. H. El-Sayed, W. Qian and M. A. El-Sayed, Journal of the American Chemical Society, 2006, **128**, 2115-2120.
29.G. Fuertes, O. L. Sanchez-Munoz, E. Pedrueza, K. Abderrafi, J. Salgado and E. Jimenez, Langmuir, 2011, **27**, 2826-2833.
30.N. Narband, M. Uppal, C. W. Dunnill, G. Hyett, M. Wilson and I. P. Parkin, Physical Chemistry Chemical Physics, 2009, **11**, 10513-10518.
31.T. Ming, L. Zhao, Z. Yang, H. J. Chen, L. D. Sun, J. F. Wang and C. H. Yan, Nano Letters, 2009, **9**, 3896-3903.
32.C. K. Tsung, X. S. Kou, Q. H. Shi, J. P. Zhang, M. H. Yeung, J. F. Wang and G. D. Stucky, Journal of the American Chemical Society, 2006, **128**, 5352-5353.
33.C. Fernandez-Lopez, C. Mateo-Mateo, R. A. Alvarez-Puebla, J. Perez-Juste, I. Pastoriza-Santos and L. M. Liz-Marzan, Langmuir, 2009, **25**, 13894-13899.
34.C. J. Orendorff and C. J. Murphy, Journal of Physical Chemistry B, 2006, **110**, 3990-3994.
35.E. Dahlstedt, H. A. Collins, M. Balaz, M. K. Kuimova, M. Khurana, B. C. Wilson, D. Phillips and H. L. Anderson, Organic & Biomolecular Chemistry, 2009, **7**, 897-904.